

# Sullivan process near threshold and the pion gravitational form factors

Yoshitaka Hatta and Jakob Schoenleber

*Physics Department, Brookhaven National Laboratory, Upton, NY 11973, USA and  
RIKEN BNL Research Center, Brookhaven National Laboratory, Upton, NY 11973, USA*

We propose a novel method to experimentally access the gravitational form factors (GFFs) of the charged pion  $\pi^+$  through the Sullivan process in electron-proton scattering. We demonstrate that the cross sections of  $J/\psi$ -photoproduction and  $\phi$ -electroproduction near the respective thresholds are dominated by the gluon GFF of the pion to next-to-leading order in perturbative QCD. We predict cross sections for the Electron-Ion Collider and the Jefferson Lab experiments.

*Introduction*—Recently, exclusive photoproduction of heavy vector mesons such as  $J/\psi$  and  $\Upsilon$  near threshold has emerged as a promising tool to access the nucleon gravitational form factors (GFFs) defined as the off-forward matrix elements of the QCD energy momentum tensor  $\langle p'|T^{\mu\nu}|p\rangle$  [1–15] [16–19]. This is complementary to the ‘canonical’ approach based on the extraction of the generalized parton distributions (GPDs) from deeply virtual Compton scattering (DVCS) [20–23]. The major challenge of GPD-based approaches is to isolate the contribution of the spin-2 energy momentum tensor from infinitely many leading twist operators with different spins. This problem can be mitigated in near-threshold productions characterized by large values of the skewness variable  $\xi \sim \mathcal{O}(1)$ . In this kinematical region, the sensitivity to the spin-2 component is significantly enhanced [7, 8, 11] compared to the situation in high energy processes with  $\xi \ll 1$ . This paves the way to efficiently access the nucleon’s gluon GFFs.

Importantly, one can realize the situation  $\xi \sim \mathcal{O}(1)$  in the electroproduction of light vector mesons near threshold where the photon virtuality  $Q^2$  serves as the hard scale for GPD factorization [7]. The case with  $\phi$ -production off the nucleon is studied in a separate publication [14], where it is demonstrated to next-to-leading order (NLO) in perturbative QCD that the cross section is dominated by the gluon and strangeness GFFs.

In this paper, for the first time we explore the physics of near-threshold vector meson productions off the charged pion  $\pi^+$ , with the goal of constraining the pion GFFs. The GFFs of the pion are of special interest due to the unique nature of the pion as the Nambu-Goldstone bosons of spontaneously broken chiral symmetry. The soft pion theorem imposes various constraints on the GFFs and even GPDs [24–26] which could be experimentally tested. While there has been a recent surge of interest in computing the pion GFFs in various approaches [27–35], attempts to extract the pion GFFs from experimental data are quite limited [27]. We shall demonstrate that the new observables considered here have very good sensitivities to the pion GFFs, and make predictions for future experiments at Jefferson Laboratory (JLab) [36] and the Electron-Ion Collider (EIC) at Brookhaven National Laboratory [37].

*Exclusive vector meson production in Sullivan process*—The Sullivan process [38] collectively refers

to a subset of electron-proton  $e + p$  scattering events where the incoming proton transitions into a neutron by emitting a virtual pion  $p(p) \rightarrow \pi^{+*}(p_\pi) + n(p_n)$  with virtuality  $p_\pi^2 = (p - p_n)^2 = t < 0$ , see Fig. 1. The pion then interacts with a virtual photon emitted from the electron  $e(l) \rightarrow \gamma^*(q) + e(l')$  with virtuality  $q^2 = (l - l')^2 = -Q^2 \leq 0$ . Depending on subsequent  $\gamma^* + \pi^{+*}$  reactions, different aspects of the pion structure can be studied [39]. In the context of the pion GPDs, previous works focused on Deeply Virtual Compton Scattering (DVCS)  $\gamma^*(q) + \pi^{+*}(p_\pi) \rightarrow \gamma(q') + \pi^+(p'_\pi)$  at high center-of-mass energy  $s_\pi = (p_\pi + q)^2 \sim Q^2$  [40, 41]. There one encounters the usual complications such as the interference with the Bethe-Heitler process and the deconvolution problem of GPDs. In this work, we instead study two exclusive processes: (i) Deeply Virtual Meson Production (DVMP)  $\gamma^*(q) + \pi^{+*}(p_\pi) \rightarrow V(q') + \pi^+(p'_\pi)$  where  $Q^2 \gg \Lambda_{\text{QCD}}^2$  and  $V$  is a neutral, longitudinally polarized light vector meson such as  $\rho^0(770)$ ,  $\omega(783)$  or  $\phi(1020)$ . (ii) Photoproduction ( $Q^2 = 0$ ) of  $J/\psi(3097)$ . The necessary hard scale for GPD factorization is provided by  $Q^2$  in the former and the  $J/\psi$  mass in the latter. The novelty of our work is that we analyze these processes in the threshold region

$$s_\pi \gtrsim s_\pi^{\text{th}} \equiv (m_\pi + m_V)^2. \quad (1)$$

Some caveats regarding the application of factorization

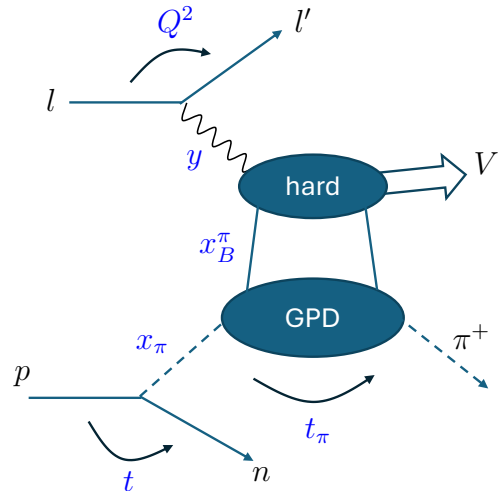


FIG. 1: Vector meson production in Sullivan process.

theorems to the threshold region has been discussed in [8, 14] for the nucleon target. For the pion target, these caveats are less significant due to the light pion mass. A more serious problem may be that the incoming pion is virtual. However, as long as  $p_\pi^2 = t$  is small, the impact on the pion GPDs is expected to be minor [39] and can be theoretically taken into account [42]. Assuming this to be the case, our goal is to assess to what extent the scattering amplitudes are sensitive to the pion GFFs.

Let us first consider DVMP. We introduce the momentum fraction  $x_\pi$  of the proton carried by the pion and the Bjorken variable  $x_B^\pi$  for the  $\gamma^* + \pi^{+\ast}$  subprocess

$$x_\pi = \frac{p_\pi \cdot l}{p \cdot l}, \quad x_B^\pi = \frac{Q^2}{2p_\pi \cdot q}. \quad (2)$$

In the limit  $Q^2 \rightarrow \infty$ , the usual Bjorken variable  $x_B$  factorizes as [40]

$$x_B = \frac{Q^2}{2p \cdot q} \approx x_\pi x_B^\pi. \quad (3)$$

At low-energy, near the threshold  $s_\pi^{th} \lesssim s_\pi \ll Q^2$ , an additional condition  $x_B^\pi \approx 1$  follows from the relation

$$s_\pi = Q^2 \left( \frac{1}{x_B^\pi} - 1 \right) + t. \quad (4)$$

Therefore, the threshold region sits along the diagonal line  $x_B \approx x_\pi$  in the  $(x_\pi, x_B)$  plane. There the skewness variable is order unity

$$\xi \approx \frac{x_B^\pi}{2 - x_B^\pi \left( 1 - \frac{t_\pi}{Q^2} \right)} \approx \frac{x_B}{2x_\pi - x_B \left( 1 - \frac{t_\pi}{Q^2} \right)} \sim \mathcal{O}(1), \quad (5)$$

where we ignored  $\mathcal{O}(1/Q^2)$  terms except for the dependence on the pion momentum transfer  $t_\pi = (p_\pi - p'_\pi)^2$  which can become large in actual experiments. This is plotted in Fig. 2. The ranges of  $x_\pi, x_B$  depend on  $s_{ep} = (p + l)^2$  and the upper cutoff  $|t| < |t_{max}|$  [38, 40], see the Supplemental Material. Working in the small- $x_\pi$  region helps to avoid the  $\Delta$ -resonance region  $M_{\pi n}^2 = (p_n + p'_\pi)^2 \sim 1.5 \text{ GeV}^2$  [40].

In the case of  $J/\psi$  photoproduction  $Q^2 = 0$ , we remove the electron vertex and consider the reduced cross section  $\gamma + p \rightarrow J/\psi + \pi^+ + n$ . Again,  $\xi$  becomes order unity near the threshold  $s_\pi \gtrsim (m_\pi + m_{J/\psi})^2 \approx 10.5 \text{ GeV}^2$ . It is important to note that, due to the light pion mass,  $\xi$  can be tuned closer to unity for the pion target than for the nucleon target in both processes.

*Threshold approximation*—The basic ingredients of the QCD factorization approach are the convolution integrals of GPDs. To leading order they have the form

$$\mathcal{H}^a(\xi, t, \mu^2) = \int_{-1}^1 dx \frac{1}{\xi - x - i\epsilon} \left\{ \frac{1}{2} H^{q(+)}(x, \xi, t, \mu^2) + \frac{1}{x} H^g(x, \xi, t, \mu^2) \right\} \quad (6)$$

where  $q = u, d, s, \dots$  is the flavor label and  $H^{q(+)}(x, \xi) = H^q(x, \xi) - H^q(-x, \xi)$  is the C-even part.  $\mu^2$  is the renormalization scale. Typically, at high energy  $s_\pi \gg Q^2$

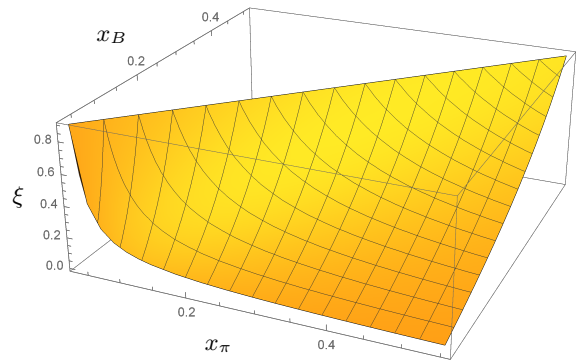


FIG. 2: Skewness  $\xi$  (5) in the  $(x_\pi, x_B)$  plane at  $\sqrt{s_{ep}} = 20 \text{ GeV}$ ,  $Q^2 = 10 \text{ GeV}^2$ ,  $t_\pi = -0.5 \text{ GeV}^2$ .

where  $\xi \ll 1$ , one tries to extract GPDs  $H$  from  $\mathcal{H}$  by deconvoluting the  $x$ -integral. However, it has been originally observed in [7, 8] and further refined in [11] that, when  $\xi \sim \mathcal{O}(1)$  and for the gluon channel  $a = g$ , (6) can be well approximated by

$$\mathcal{H}_{\text{trunc}}^a(\xi, t, \mu^2) = \frac{2}{\xi^2} \frac{5}{4} (A^a(t, \mu^2) + \xi^2 D^a(t, \mu^2)), \quad (7)$$

where  $A, D$  are the gravitational form factors

$$A^a(t, \mu^2) + \xi^2 D^a(t, \mu^2) = \int_{-1}^1 dx \left\{ x H^a(x, \xi, t, \mu^2) + \frac{1}{2} H^g(x, \xi, t, \mu^2) \right\} \quad (8)$$

(7) is nothing but the leading order term in the conformal partial wave expansion [43, 44] of (6). Drastic as it may seem, the validity of this ‘threshold approximation’ for the nucleon target has been tested to next-to-leading order (NLO) in  $\phi$ -electroproduction [14] and  $J/\psi$ -photoproduction [15]. The approximation works fine already for moderately large values  $\xi \gtrsim 0.4$ . Below we test this approach for the pion target.

For this purpose, we adopt the ‘algebraic’ model of the pion GPDs  $H_\pi^a(x, \xi, t_\pi, \mu^2)$  constructed in [26]. In the Supplemental Material, we discuss another model to check the model dependence. A notable feature of this model is that it contains the so-called D-term [45] which has support in the central region  $|x| < \xi$

$$H_\pi^a(x, \xi, t_\pi, \mu^2) \sim \theta(\xi - |x|) D_\pi^a(x/\xi, t_\pi, \mu^2). \quad (9)$$

Remarkably, in the chiral limit of QCD, the forward value  $D_\pi^a(x/\xi, t_\pi = 0)$  is strongly constrained by the soft pion theorem for all parton species  $a = q, g$  [25, 26]. This in particular means that

$$D_\pi^q(0, \mu^2) = \int_{-1}^1 dz z D_\pi^q(z, 0, \mu^2) = -A_\pi^q(0, \mu^2), \quad (10)$$

and similarly for the gluon. The model also assumes isospin symmetry which means  $H_\pi^{u(+)}(x, \xi, t_\pi) = H_\pi^{d(+)}(x, \xi, t_\pi)$  exactly. In real QCD, there are deviations from these relations.

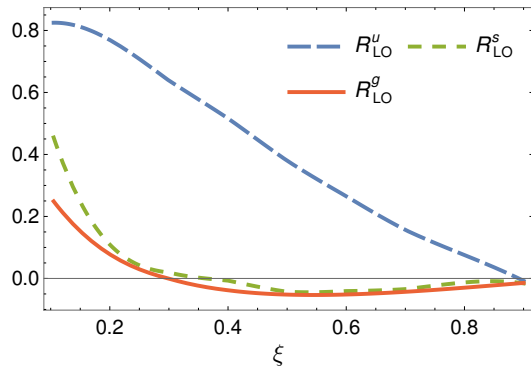


FIG. 3: Truncation error  $R^{a=u,s,g}$  (11) of the leading order amplitude (6) at  $\mu^2 = 10 \text{ GeV}^2$ .

Using the algebraic model evolved to  $\mu^2 = 10 \text{ GeV}^2$  and setting  $t_\pi = 0$  for simplicity, we numerically evaluate (6) and compare the results with their truncated versions (7). This is plotted in Fig. 3 in terms of the ratio

$$R_f^a(\xi) = 1 - \frac{\sqrt{(\text{Re } \mathcal{H}_f^a)^2 + (\text{Im } \mathcal{H}_f^a)^2}}{\mathcal{H}_{f,\text{trunc}}^a}, \quad (11)$$

which is the measure of the truncation error. The index  $f = \text{LO}, \text{NLO}$  denotes whether the leading order or next-to-leading order hard kernel has been used. We immediately notice that the approximation fails for  $u, d$  quarks, which are important for  $\rho^0, \omega$ -productions, unless one reaches  $\xi \gtrsim 0.7$ . The main reason is that the corresponding GPD is well supported in the DGLAP region  $\xi < |x| < 1$  and takes a sizable value at the diagonal point  $x = \xi$ , giving rise to a large imaginary part  $\text{Im } \mathcal{H}_\pi^{u,d}(\xi) \propto H_\pi^{u,d}(\xi, \xi)$ . This is related to the fact that  $u, d$  quarks constitute the valence quarks of the  $\pi^+$ . In the asymptotic limit  $\mu^2 \rightarrow \infty$ ,  $H_\pi^{u,d}(\xi, \xi, \mu^2)$  should go to zero and the threshold approximation becomes exact. But this occurs at much higher scales than  $\mu^2 = 10 \text{ GeV}^2$  in the present model.

On the other hand, the approximation works very well in the gluon and strangeness channels. The truncation error is less than 10% already for  $\xi > 0.2$ . In contrast to  $H_\pi^{u,d}$ ,  $H_\pi^{s,g}$  are dominantly supported in the central region  $|x| < \xi$ , leading to a small imaginary part in the amplitude  $\text{Im } \mathcal{H}_\pi^{s,g}(\xi) \propto H_\pi^{s,g}(\xi, \xi)$ . We therefore focus on  $\phi$ -electroproduction and  $J/\psi$ -photoproduction in what follows and test the validity of the threshold approximation to NLO. For  $\phi$ -electroproduction, we use the full NLO scattering amplitude from [44, 46, 47], and its truncated version in [14]. In the  $J/\psi$  case, we use the full NLO result from [48] and its truncated version [15].

The results for  $R_{\text{NLO}}$  are plotted in Fig. 4. Each plot shows  $R_{\text{NLO}}$  for different partonic channels  $a = g, s, ps$  where  $ps$  means the ‘pure singlet’ contribution (the sum of GPDs/GFFs over all flavors) that appears at NLO. The total NLO amplitude is indicated by the solid line. The threshold approximation is excellent  $|R_{\text{NLO}}^\phi| < 0.05$

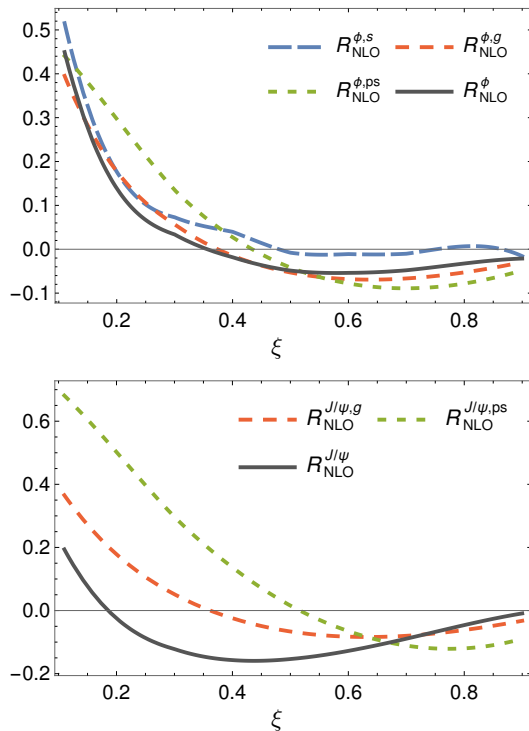


FIG. 4: Truncation error (11) in the full NLO amplitude at  $\mu^2 = 10 \text{ GeV}^2$ . Top:  $\phi$ -electroproduction. Bottom:  $J/\psi$ -photoproduction.

for  $\phi$ -electroproduction at  $\mu^2 = 10 \text{ GeV}^2 = Q^2$  (upper plot). As for  $J/\psi$ -photoproduction, the approximation is not as good as in the  $\phi$ -production case due to the partial cancellation between the quark and gluon terms. Still, it is decent  $|R_{\text{NLO}}^{J/\psi}| < 0.2$  and increasingly gets better as  $\xi \rightarrow 1$ .

*Predictions at the EIC and JLab*—Now that we have demonstrated the validity of the threshold approximation for  $\phi$ -electroproduction and  $J/\psi$ -photoproduction, we make concrete NLO predictions for the JLab and EIC kinematics. The relevant cross section formulas are summarized in the Supplemental Material. We assume the monopole and dipole form for the  $A, D$  form factors [28] (see also [29])

$$A_\pi^a(t, \mu^2) = \frac{A_\pi^a(0, \mu^2)}{1 - t/m_A^2}, \quad D_\pi^a(t, \mu^2) = \frac{D_\pi^a(0, \mu^2)}{(1 - t/m_D^2)^2}. \quad (12)$$

We use  $m_A = 1.6 \text{ GeV}$  and  $m_D = 1.1 \text{ GeV}$  as in [14], but ultimately these parameters should be determined from future experimental data. The forward values  $A_\pi^a(0, \mu^2)$  are constrained by the pion PDF. We use  $A_\pi^u = A_\pi^d = 0.28$  (isospin symmetry),  $A_\pi^s = 0.02$  and  $A_\pi^g = 0.41$  at the reference scale  $\mu^2 = 2 \text{ GeV}^2$  from the algebraic model and consider their one-loop evolution with  $n_f = 4$  flavors. We impose the constraint  $D_\pi^a(0, \mu^2) = -A_\pi^a(0, \mu^2)$  from the soft pion theorem, although possible deviations from this formula are interesting and can be implemented in a straightforward manner.

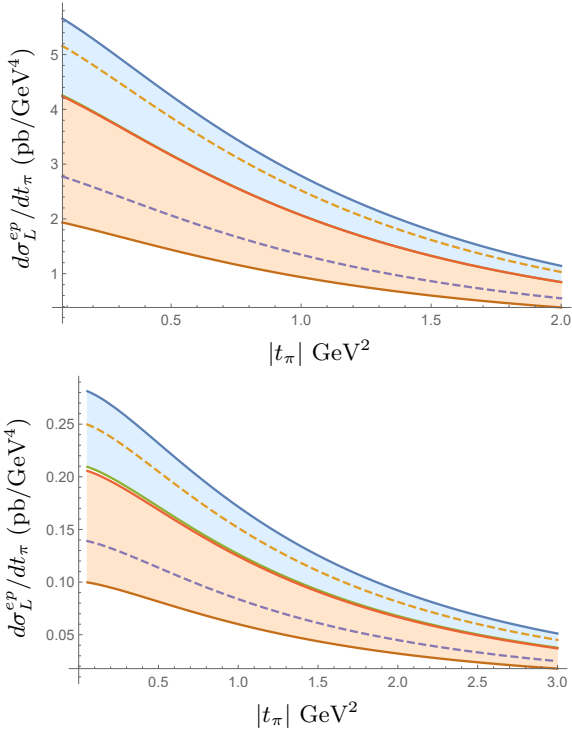


FIG. 5: Longitudinal part of the  $ep$  cross section (13) at  $x_\pi = 0.3$ ,  $x_B = 0.2$  as a function of  $|t_\pi|$ . Top:  $Q^2 = 5 \text{ GeV}^2$ , Bottom:  $Q^2 = 10 \text{ GeV}^2$ . Blue and orange band are the NLO and LO cross sections, respectively, varied within  $Q/2 < \mu < 2Q$ .

First consider  $\phi$ -electroproduction at the EIC with  $\sqrt{s_{ep}} = 20 \text{ GeV}$ . We write the  $e + p$  cross section as (not to be confused with the reduced  $\gamma^* + p$  cross section  $d\sigma_{T/L}^{\gamma^* p}$ )

$$\frac{d\sigma^{ep}}{dx_B dQ^2 dt_\pi dx_\pi} \equiv \frac{d\sigma_T^{ep}}{dx_B dQ^2 dt_\pi dx_\pi} + \varepsilon \frac{d\sigma_L^{ep}}{dx_B dQ^2 dt_\pi dx_\pi}, \quad (13)$$

where the longitudinal/transverse photon flux ratio  $\varepsilon$  is

$$\varepsilon = \frac{1 - y_\pi}{1 - y_\pi + \frac{y_\pi^2}{2}}, \quad y_\pi = \frac{q \cdot p_\pi}{l \cdot p_\pi}. \quad (14)$$

In the present kinematics,  $y_\pi$  is approximately equal to the usual DIS variable  $y$  [40]

$$y_\pi \approx y = \frac{q \cdot p}{l \cdot p} = \frac{Q^2}{(s_{ep} - m_N^2)x_B}, \quad (15)$$

where  $m_N$  is the nucleon mass. We focus on the longitudinal part  $d\sigma_L^{ep}$  which admits QCD factorization [49]. Fig. 5 shows  $d\sigma_L^{ep}$  evaluated at a representative point  $(x_\pi, x_B) = (0.3, 0.2)$  with two different values  $Q^2 = 5 \text{ GeV}^2$  (top) and  $Q^2 = 10 \text{ GeV}^2$  (bottom). The NLO cross section (blue band) is larger and has smaller scale uncertainties than the LO cross section (orange band).

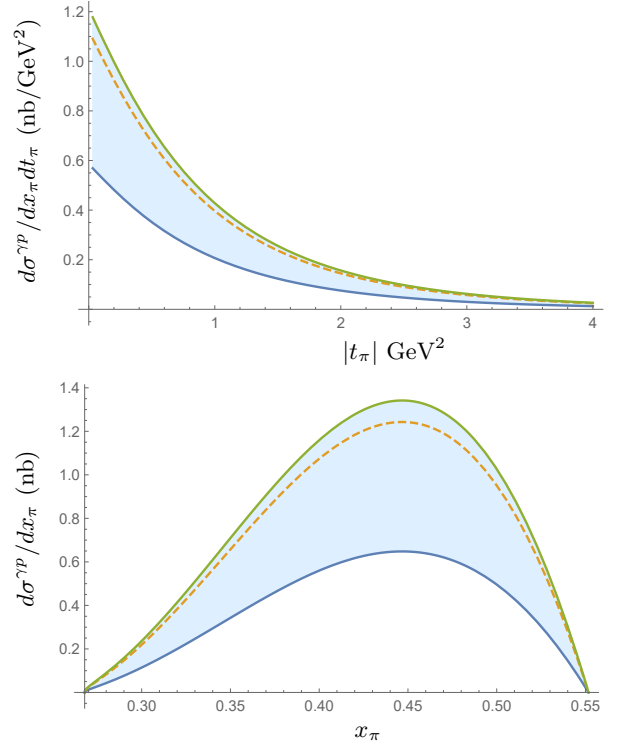


FIG. 6: Upper plot:  $J/\psi$ -photoproduction cross section (16) at JLab with  $s_{\gamma p} = 40 \text{ GeV}^2$  and  $x_\pi = 0.4$ . Lower plot: Cross section integrated over  $t_\pi$ . The three curves correspond to  $\mu = 2m_{J/\psi}, m_{J/\psi}$  and  $m_{J/\psi}/2$  from top to bottom.

In these plots,  $\xi > 0.5$ , where the truncation error (see Fig. 4) is expected to be smaller than the scale uncertainties and possible higher twist effects of order  $t_\pi/Q^2$ . The cross section is dominated by the gluon exchange which is partly canceled by the NLO quark contribution. Because of the soft pion theorem  $D_\pi^s(0) \approx -A_\pi^s(0)$ , the large- $D_s$  scenario for the nucleon considered in [7, 14] is unlikely for the pion. The rather weak  $t_\pi$ -dependence is due to the monopole ansatz (12) which can be experimentally tested.

The corresponding measurement at JLab will be more difficult, as the allowed ranges of  $x_\pi, x_B$  are narrower at the current JLab energy  $s_{ep} \approx 23 \text{ GeV}^2$ . One is forced to go to lower regions in  $Q^2$  at the risk of reducing the accuracy of perturbative predictions. The proposed 22 GeV upgrade ( $s_{ep} \approx 42 \text{ GeV}^2$ ) [50], if realized, certainly improves the situation. The Electron-Ion Collider in China (EIC) [51] offers another possibility. One advantage of low energy experiments is that it may be possible to perform the longitudinal/transverse (L/T) decomposition via the ‘Rosenbluth separation’ method. Usually, one varies  $\varepsilon$  by changing the beam energy  $s_{ep}$  at fixed  $Q^2, x_B$  (see (15)). But in the Sullivan process, one may as well fix  $s_{ep}$  and vary  $x_B$  along the ‘degenerate’ line  $x_B^\pi \approx x_B/x_\pi = \text{const}$ . This allows one to access the low- $\varepsilon$  region critical for the method [52].

Next we consider  $J/\psi$ -photoproduction at JLab. We

compute the reduced  $\gamma + p$  cross section

$$\frac{d\sigma^{\gamma p}}{dx_\pi dt_\pi}, \quad (16)$$

treating the photon energy  $q^0 = E_\gamma$  as a fixed parameter. This can be controllably done as in the recent JLab measurements of  $J/\psi$  off the nucleon target [16–18]. However, the same is challenging for the pion target in the Sullivan process due to the lack of phase space (S19). We thus assume the 22 GeV upgrade [50] and fix  $s_{\gamma p} = (q + p)^2 = 40 \text{ GeV}^2$ . In Fig. 6, we plot (16) at  $x_\pi = 0.4$  corresponding to  $\xi > 0.44$ . The uncertainty band suggests that the natural scale is  $\mu = m_{J/\psi}$  or even higher, rather than the charm quark mass  $\mu = m_{J/\psi}/2$ . The magnitude of the cross section is of the same order as in the nucleon target production [16–18] and falls slower with  $|t_\pi|$ . The lower plot is the  $t_\pi$ -integrated cross section which clearly shows the rise of the cross section above the threshold  $x_\pi > 0.27$ . The upper limit  $x_\pi \lesssim 0.55$  is an artificial cutoff imposed by the condition  $|t| < |t_{max}| = 0.6 \text{ GeV}^2$  [40, 53].

*Conclusions*—In this paper we have proposed a novel method to experimentally constrain the gluon and strangeness gravitational form factors of the pion. We have demonstrated to NLO in QCD that  $\phi$ -electroproduction and  $J/\psi$ -photoproduction near the threshold have strong sensitivities to the pion GFFs. Moreover, thanks to the light pion mass, one can explore larger  $\xi$  and lower  $|t_\pi|$  regions than for the nucleon target, which makes theoretical treatments cleaner. The

predicted NLO cross sections are well in the measurable range with the high luminosities of the EIC and JLab.

There are many directions for future exploration. First, it would be interesting to further investigate the sensitivity of near-threshold  $\rho^0$  and  $\omega$ -productions to the up and down quark GFFs. The region  $\xi > 0.7$  (see Fig. 3) is not inaccessible for the pion target, but there are practical issues such as model dependence and experimental feasibility. Second, while near-threshold photoproduction is challenging to measure at the EIC, electroproduction of  $J/\psi$  should be possible [5]. The calculation can be pushed to NLO using the result of [54]. One can also consider photoproduction in proton-nucleus ultraperipheral collisions (UPCs) [2]. The Sullivan process in these reactions has not been discussed in the literature. Finally, the need for reconstructing the scattered particles  $e, V, \pi^+, n$  poses significant experimental challenges. Careful investigations based on realistic experimental setups and event generator simulations (see, e.g., [14]) are crucial in this respect. We hope our work triggers future efforts in this direction.

*Acknowledgments*—We thank Henry Klest and Kornelija Passek-K. for the collaboration in [14] and discussions on various aspects of this work. We also thank Jose Morgado-Chavez and Cedric Mezrag for numerical tables of the GPD models in [26]. We were supported by the U.S. Department of Energy under Contract No. DE-SC0012704, and also by LDRD funds from Brookhaven Science Associates.

- 
- [1] Y. Hatta and D.-L. Yang, Phys. Rev. D **98**, 074003 (2018), 1808.02163.
- [2] Y. Hatta, A. Rajan, and D.-L. Yang, Phys. Rev. D **100**, 014032 (2019), 1906.00894.
- [3] K. A. Mamo and I. Zahed, Phys. Rev. D **101**, 086003 (2020), 1910.04707.
- [4] R. Wang, J. Evslin, and X. Chen, Eur. Phys. J. C **80**, 507 (2020), 1912.12040.
- [5] R. Boussarie and Y. Hatta, Phys. Rev. D **101**, 114004 (2020), 2004.12715.
- [6] D. E. Kharzeev, Phys. Rev. D **104**, 054015 (2021), 2102.00110.
- [7] Y. Hatta and M. Strikman, Phys. Lett. B **817**, 136295 (2021), 2102.12631.
- [8] Y. Guo, X. Ji, and Y. Liu, Phys. Rev. D **103**, 096010 (2021), 2103.11506.
- [9] K. A. Mamo and I. Zahed, Phys. Rev. D **103**, 094010 (2021), 2103.03186.
- [10] P. Sun, X.-B. Tong, and F. Yuan, Phys. Rev. D **105**, 054032 (2022), 2111.07034.
- [11] Y. Guo, X. Ji, and F. Yuan, Phys. Rev. D **109**, 014014 (2024), 2308.13006.
- [12] X.-Y. Wang and J. Bu, Phys. Rev. C **110**, 025206 (2024), 2402.05354.
- [13] L. Pentchev and E. Chudakov (2024), 2404.18776.
- [14] Y. Hatta, H. T. Klest, K. Passek-K., and J. Schoenleber (2025), 2501.12343.
- [15] Y. Guo, F. Yuan, and W. Zhao (2025), 2501.10532.
- [16] A. Ali et al. (GlueX), Phys. Rev. Lett. **123**, 072001 (2019), 1905.10811.
- [17] B. Duran et al., Nature **615**, 813 (2023), 2207.05212.
- [18] S. Adhikari et al. (GlueX), Phys. Rev. C **108**, 025201 (2023), 2304.03845.
- [19] H. T. Klest et al. (2025), 2501.01582.
- [20] I. V. Anikin and O. V. Teryaev, Phys. Rev. D **76**, 056007 (2007), 0704.2185.
- [21] V. D. Burkert, L. Elouadrhiri, and F. X. Girod, Nature **557**, 396 (2018).
- [22] K. Kumerički, Nature **570**, E1 (2019).
- [23] H. Dutrieux, T. Meisgny, C. Mezrag, and H. Moutarde (2024), 2410.13518.
- [24] V. A. Novikov and M. A. Shifman, Z. Phys. C **8**, 43 (1981).
- [25] M. V. Polyakov, Nucl. Phys. B **555**, 231 (1999), hep-ph/9809483.
- [26] J. M. M. Chavez, V. Bertone, F. De Soto Borrero, M. Defurne, C. Mezrag, H. Moutarde, J. Rodríguez-Quintero, and J. Segovia, Phys. Rev. D **105**, 094012 (2022), 2110.06052.
- [27] S. Kumano, Q.-T. Song, and O. V. Teryaev, Phys. Rev. D **97**, 014020 (2018), 1711.08088.
- [28] K. Tanaka, Phys. Rev. D **98**, 034009 (2018), 1806.10591.

- [29] X.-B. Tong, J.-P. Ma, and F. Yuan, Phys. Lett. B **823**, 136751 (2021), 2101.02395.
- [30] D. C. Hackett, P. R. Oare, D. A. Pefkou, and P. E. Shanahan, Phys. Rev. D **108**, 114504 (2023), 2307.11707.
- [31] Y.-Z. Xu, M. Ding, K. Raya, C. D. Roberts, J. Rodríguez-Quintero, and S. M. Schmidt, Eur. Phys. J. C **84**, 191 (2024), 2311.14832.
- [32] B. Wang, F. He, G. Wang, T. Draper, J. Liang, K.-F. Liu, and Y.-B. Yang ( $\chi$ QCD), Phys. Rev. D **109**, 094504 (2024), 2401.05496.
- [33] D. Fujii, A. Iwanaka, and M. Tanaka, Phys. Rev. D **110**, L091501 (2024), 2407.21113.
- [34] W. Broniowski and E. Ruiz Arriola, Phys. Lett. B **859**, 139138 (2024), 2405.07815.
- [35] W.-Y. Liu, E. Shuryak, C. Weiss, and I. Zahed, Phys. Rev. D **110**, 054021 (2024), 2405.14026.
- [36] J. Arrington et al. (Jefferson Lab SoLID), J. Phys. G **50**, 110501 (2023), 2209.13357.
- [37] R. Abdul Khalek et al., Nucl. Phys. A **1026**, 122447 (2022), 2103.05419.
- [38] J. D. Sullivan, Phys. Rev. D **5**, 1732 (1972).
- [39] A. C. Aguilar et al., Eur. Phys. J. A **55**, 190 (2019), 1907.08218.
- [40] D. Amrath, M. Diehl, and J.-P. Lansberg, Eur. Phys. J. C **58**, 179 (2008), 0807.4474.
- [41] J. M. M. Chávez, V. Bertone, M. Defurne, F. de Soto, C. Mezrag, H. Moutarde, J. Rodríguez-Quintero, and J. Segovia, Rev. Mex. Fis. Suppl. **3**, 0308099 (2022), 2203.16947.
- [42] W. Broniowski, V. Shastry, and E. Ruiz Arriola, Phys. Lett. B **840**, 137872 (2023), 2211.11067.
- [43] D. Mueller and A. Schafer, Nucl. Phys. B **739**, 1 (2006), hep-ph/0509204.
- [44] D. Müller, T. Lautenschlager, K. Passek-Kumericki, and A. Schaefer, Nucl. Phys. B **884**, 438 (2014), 1310.5394.
- [45] M. V. Polyakov and C. Weiss, Phys. Rev. D **60**, 114017 (1999), hep-ph/9902451.
- [46] G. Duplancić, D. Müller, and K. Passek-Kumerički, Phys. Lett. B **771**, 603 (2017), 1612.01937.
- [47] M. Čuić, G. Duplancić, K. Kumerički, and K. Passek-K., JHEP **12**, 192 (2023), [Erratum: JHEP 02, 225 (2024)], 2310.13837.
- [48] D. Y. Ivanov, A. Schafer, L. Szymanowski, and G. Krasnikov, Eur. Phys. J. C **34**, 297 (2004), [Erratum: Eur.Phys.J.C 75, 75 (2015)], hep-ph/0401131.
- [49] J. C. Collins, L. Frankfurt, and M. Strikman, Phys. Rev. D **56**, 2982 (1997), hep-ph/9611433.
- [50] A. Accardi et al., Eur. Phys. J. A **60**, 173 (2024), 2306.09360.
- [51] D. P. Anderle et al., Front. Phys. (Beijing) **16**, 64701 (2021), 2102.09222.
- [52] H. P. Blok et al. (Jefferson Lab), Phys. Rev. C **78**, 045202 (2008), 0809.3161.
- [53] S.-X. Qin, C. Chen, C. Mezrag, and C. D. Roberts, Phys. Rev. C **97**, 015203 (2018), 1702.06100.
- [54] C. A. Flett, J. A. Gracey, S. P. Jones, and T. Teubner, JHEP **08**, 150 (2021), 2105.07657.

---

## Supplemental Materials

### I. KINEMATICS AND CROSS SECTION FORMULAS

#### A. Meson electroproduction

Here we review the kinematics of DVMP in the Sullivan process building on [38, 40]. We introduce the usual DIS variables

$$s_{ep} = (p + l)^2, \quad x_B = \frac{Q^2}{2p \cdot q}, \quad y = \frac{q \cdot p}{l \cdot p} \quad (S1)$$

and their counterparts in the  $e + \pi^{+*}$  subprocess

$$x_B^\pi = \frac{Q^2}{2p_\pi \cdot q}, \quad y_\pi = \frac{q \cdot p_\pi}{l \cdot p_\pi}. \quad (S2)$$

where  $p_\pi = p - n$ , see Fig. 1. We treat the electron as massless. The other important variables are the momentum fraction  $x_\pi$  of the proton carried by the pion and the momentum transfer  $t_\pi$  in the subsequent scattering  $\gamma^*(q) + \pi^{+*}(p_\pi) \rightarrow V + \pi^+(p'_\pi)$

$$x_\pi = \frac{p_\pi \cdot l}{p \cdot l}, \quad t_\pi = (p_\pi - p'_\pi)^2. \quad (S3)$$

In the  $Q^2 \rightarrow \infty$  limit, one generically has [40]

$$x_B^\pi \approx \frac{x_B}{x_\pi}, \quad y_\pi \approx y = \frac{Q^2}{(s_{ep} - m_N^2)x_B}. \quad (S4)$$

The nucleon momentum transfer  $t = p_\pi^2$  is restricted to

$$|t_{min}| = \frac{x_\pi^2 m_N^2}{1 - x_\pi} < |t| < |t_{max}|, \quad (S5)$$

The lower limit is a kinematical constraint. The upper limit  $t_{max}$  ensures that the transition  $p \rightarrow n$  is dominated by the one-pion emission. Typically  $|t| \ll 1 \text{ GeV}^2$ , but we allow for  $|t_{max}| = 0.6 \text{ GeV}^2$  [40, 53]. The range of  $x_\pi$  is

$$\frac{s_\pi^{th} + Q^2}{(s_{ep} - m_N^2)y_{max}} \lesssim x_\pi < \frac{-|t_{max}| + \sqrt{t_{max}^2 + 4|t_{max}|m_N^2}}{2m_N^2} \approx 0.55, \quad (S6)$$

where  $y_{max}$  is the maximal value of  $y$  in a given experiment. The upper limit follows from the condition  $|t_{min}| < |t_{max}|$  and the lower limit is from

$$x_\pi y \approx x_\pi y_\pi = \frac{2p_\pi \cdot q}{2p \cdot l} = \frac{s_\pi + Q^2 - t}{s_{ep} - m_N^2}. \quad (S7)$$

In principle,  $y_{max} \approx 1$ , but in practice a smaller value is adopted to suppress QED radiative corrections which become important when  $y \rightarrow 1$ . We use  $y_{max} = 0.85$ . Finally, the constraint on  $x_B$  can be deduced from the formula [40]

$$s_\pi = Q^2 \left( \frac{x_\pi}{x_B} - 1 \right) + 2yx_B x_\pi m_N^2 + (1 - yx_B)t - 2 \cos(\phi_{l'} - \phi_n) \sqrt{(1-y)Q^2 - (yx_B m_N)^2} \sqrt{(1-x_\pi)(t_{min} - t)} \quad (S8)$$

To leading order in  $Q^2$ , the cross section does not depend on the azimuthal angles  $\phi_{l'}, \phi_n, \phi_\pi$ . The cosine term can then be averaged out. Besides, from (S6),

$$x_B x_\pi m_N^2 < x_\pi^2 m_N^2 < |t_{max}|, \quad (S9)$$

is small compared to  $s_\pi > s_\pi^{th} \sim 1 \text{ GeV}^2$ . We thus find

$$\frac{Q^2}{(s_{ep} - m_N^2)y_{max}} < x_B \lesssim \min \left[ \frac{x_\pi}{1 + \frac{s_\pi^{th}}{Q^2}}, \frac{x_\pi}{1 - \frac{t_\pi}{2Q^2}} \right]. \quad (S10)$$

The second upper limit comes from the condition  $\xi < 1$  (see (5)) which is relevant only at high momentum transfer  $|t_\pi| > 2s_\pi^{th}$ .

The fully-differential  $e + p \rightarrow e' + V + \pi^+ + n$  cross section takes the form [40]

$$\frac{d\sigma^{ep}}{dydQ^2 d\phi_{l'} dt_\pi d\phi_\pi dt dx_\pi d\phi_n} = \frac{(\sqrt{2}g_{\pi NN}F(t))^2}{128(2\pi)^8 (s_{ep} - m_N^2) \sqrt{(s_\pi + Q^2 + t)^2 - 4s_\pi t} (m_\pi^2 - t)^2} \frac{-t}{|M_V(\xi, t_\pi)|^2} \quad (S11)$$

where  $g_{\pi NN} \approx 13.1$  is the pion-nucleon coupling and  $F(t)$  with  $F(m_\pi^2) = 1$  is the associated form factor. ( $\sqrt{2}$  is the isospin factor.) We decompose the hard cross section into the longitudinal and transverse parts

$$|M_V(\xi, t_\pi)|^2 = \frac{2e^4 (4\pi)^2}{Q^2 (1 - \varepsilon)} (|\mathcal{H}_V^T(\xi, t_\pi)|^2 + \varepsilon |\mathcal{H}_V^L(\xi, t_\pi)|^2) + \dots, \quad (S12)$$

where we ignore the angular dependent terms and

$$\varepsilon = \frac{1 - y_\pi}{1 - y_\pi + \frac{y_\pi^2}{2}} \approx \frac{1 - y}{1 - y + \frac{y^2}{2}}, \quad (S13)$$

is the longitudinal/transverse virtual photon flux ratio. In DVMP, only the longitudinal part is reliably calculable. In the case of  $V = \phi$ , and in the threshold approximation to NLO [14],

$$\begin{aligned} \mathcal{H}_\phi^L(\xi, t_\pi) \approx e_s \frac{C_F f_\phi}{N_c Q} \frac{2\alpha_s(\mu)}{\xi^2} \frac{15}{2} \left[ \left\{ 1 + \frac{\alpha_s}{2\pi} \left( 25.7 - 2n_f + \left( -\frac{131}{18} + \frac{n_f}{3} \right) \ln \frac{Q^2}{\mu^2} \right) \right\} (A_\pi^s(t, \mu) + \xi^2 D_\pi^s(t, \mu)) \right. \\ \left. + \frac{\alpha_s}{2\pi} \left( -2.34 + \frac{2}{3} \ln \frac{Q^2}{\mu^2} \right) \sum_q (A_\pi^q + \xi^2 D_\pi^q) + \frac{3}{8} \left\{ 1 + \frac{\alpha_s}{2\pi} \left( 13.9 - \frac{83}{18} \ln \frac{Q^2}{\mu^2} \right) \right\} (A_\pi^g + \xi^2 D_\pi^g) \right], \quad (S14) \end{aligned}$$

where  $e_s = -\frac{1}{3}$ , and  $f_\phi$  is the decay constant. We have assumed the asymptotic form  $\varphi_\phi(u) \approx 6u(1-u)$  for the meson distribution amplitude.

Returning to (S11), in the present kinematics we may approximate

$$\frac{1}{\sqrt{(s_\pi + Q^2 + t)^2 - 4s_\pi t}} \approx \frac{x_B}{x_\pi Q^2}. \quad (\text{S15})$$

We can then trivially perform all the angular integrals. As for the  $t$ -integral, we follow [40] and introduce

$$\Pi(x_\pi, t_{max}) = x_\pi \frac{g_{\pi NN}^2}{8\pi^2} \int_{t_{max}}^{t_{min}} dt F^2(t) \frac{-t}{(m_\pi^2 - t)^2}. \quad (\text{S16})$$

We use the same monopole model  $F(t) = \frac{\Lambda^2 - m_\pi^2}{\Lambda^2 - t}$  with  $\Lambda = 0.8$  GeV as in [40]. Then the  $t$ -integral can be done explicitly. Switching variables  $y \rightarrow x_B$ , we arrive at

$$\begin{aligned} \frac{d\sigma^{ep}}{dx_B dQ^2 dt_\pi dx_\pi} &= \frac{2\pi\alpha_{em}^2 \Pi(x_\pi, t_{max})}{x_\pi^2 x_B (s_{ep} - m_N^2)^2 Q^2 (1 - \varepsilon)} (|\mathcal{H}_V^T(\xi, t_\pi)|^2 + \varepsilon |\mathcal{H}_V^L(\xi, t_\pi)|^2) \\ &\equiv \frac{d\sigma_T^{ep}}{dx_B dQ^2 dt_\pi dx_\pi} + \varepsilon \frac{d\sigma_L^{ep}}{dx_B dQ^2 dt_\pi dx_\pi}. \end{aligned} \quad (\text{S17})$$

Note that  $d\sigma_L^{ep}$  still contains  $\varepsilon$  in our definition. The reader should not confuse this with the common notation  $d\sigma_{T/L}$  often used for the reduced  $\gamma^* + p$  cross section.

## B. Quarkonium photoproduction

In the case of  $J/\psi$ -photoproduction  $Q^2 = 0$  at fixed  $\gamma + p$  center-of-mass energy  $s_{\gamma p} = (p + q)^2$ , the variables  $x_B, x_B^\pi$  are not needed and  $x_\pi = \frac{p_\pi \cdot q}{p \cdot q}$ . We have the constraint

$$s_\pi = x_\pi (s_{\gamma p} - m_N^2) + t > (m_\pi + m_J)^2 \approx 10.5 \text{ GeV}^2 \quad (\text{S18})$$

which leads to

$$\frac{10.5 \text{ GeV}^2}{s_{\gamma p} - m_N^2} \lesssim x_\pi < 0.55, \quad (\text{S19})$$

where the upper limit is the same as before (S6). We define skewness as ( $v^\pm \equiv \frac{1}{\sqrt{2}}(v^0 \pm v^3)$ )

$$\xi = \frac{p_\pi^+ - p_\pi'^+}{p_\pi^+ + p_\pi'^+}, \quad (\text{S20})$$

in the  $\gamma^* + \pi^{+\ast}$  center-of-mass frame. Fig. S1 shows  $\xi$  in the  $(x_\pi, |t_\pi|)$  plane with  $s_{\gamma p} = 40 \text{ GeV}^2$  and  $t \approx 0$ . The threshold corresponds to the lower limit  $x_\pi \approx 0.27$ .

Within the non-relativistic QCD (NRQCD) framework, the differential cross section of the reduced process  $\gamma + p \rightarrow V + \pi^+ + n$  is

$$\frac{d\sigma^{\gamma p}}{dt_\pi d\phi_\pi dt dx_\pi d\phi_n} = \frac{(\sqrt{2}g_{\pi NN} F(t))^2}{32(2\pi)^5 (s_{\gamma p} - m_N^2)(s_\pi - t)} \frac{-t}{(m_\pi^2 - t)^2} 4\pi\alpha_{em} e_q^2 \frac{(16\pi)^2}{N_c m_V^3} |\psi_V(0)|^2 |\mathcal{H}_V|^2, \quad (\text{S21})$$

where  $|\psi_V(\vec{r}=0)|^2$  is the quarkonium wavefunction evaluated at the origin. For  $J/\psi$ ,  $e_q = \frac{2}{3}$  and  $|\psi(0)|^2 = 1.0952/(4\pi) \text{ GeV}^3$ . Integrating over  $t, \phi_\pi, \phi_n$ , we find

$$\frac{d\sigma^{\gamma p}}{dt_\pi dx_\pi} = 64\pi^2 \alpha_{em} e_q^2 \frac{\Pi(x_\pi, t_{max})}{x_\pi^2 (s_{\gamma p} - m_N^2)^2} \frac{|\psi_V(0)|^2}{N_c m_V^3} |\mathcal{H}_V|^2. \quad (\text{S22})$$

To leading order, the scattering amplitude is given by the gluon GPD of the pion

$$\mathcal{H}_V(\xi, t_\pi) = \alpha_s \int_{-1}^1 \frac{dx}{2x} \left( \frac{1}{\xi - x - i\epsilon} - \frac{1}{\xi + x - i\epsilon} \right) H_\pi^g(x, \xi, t_\pi) + \mathcal{O}(\alpha_s^2). \quad (\text{S23})$$

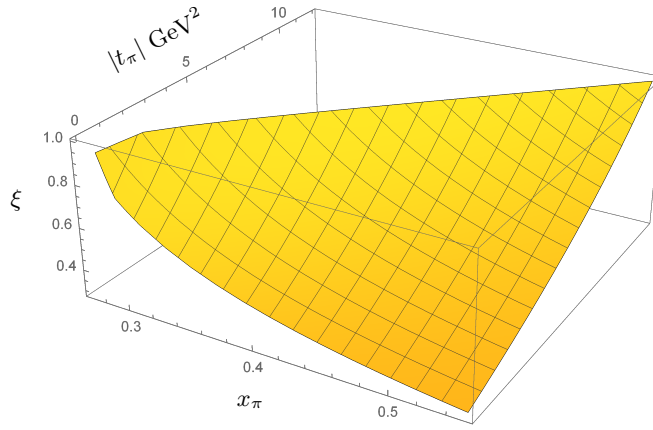


FIG. S1: Skewness in  $J/\psi$ -photoproduction at  $s_{\gamma p} = 40 \text{ GeV}^2$ .

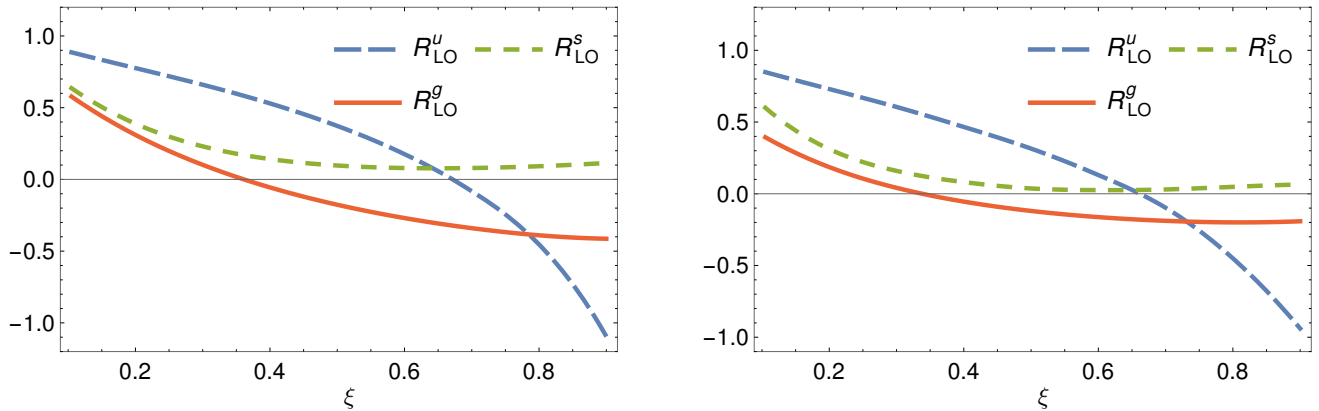


FIG. S2: Truncation error (11) of the leading order amplitude in the phenomenological model at  $\mu^2 = 2 \text{ GeV}^2$  (left) and  $\mu^2 = 10 \text{ GeV}^2$  (right).

We use the NLO  $\mathcal{O}(\alpha_s^2)$  result from [48]. In the threshold approximation, this reduces to [15]

$$\mathcal{H}_{\text{trunc}}(\xi) = \frac{2\alpha_s(\mu)}{\xi^2} \frac{5}{4} \left[ \left( 1 + \frac{\alpha_s}{2\pi} \left( 5.77 - \frac{11}{2} \ln \frac{4m_c^2}{\mu^2} \right) \right) (A_\pi^g + \xi^2 D_\pi^g) + \frac{\alpha_s}{2\pi} \left( -6.94 + \frac{16}{9} \ln \frac{4m_c^2}{\mu^2} \right) \sum_q (A_\pi^q + \xi^2 D_\pi^q) \right], \quad (\text{S24})$$

where  $m_c \approx m_{J/\psi}/2$  is the charm quark mass. Note that this is renormalization group invariant up to terms of order  $\mathcal{O}(\alpha_s^3)$ . In practice, we observe a strong  $\mu$ -dependence around  $\mu = m_c$  due to a cancellation between the quark and gluon terms. On the other hand, the amplitude shows a stable plateau in the window  $2m_c \approx m_{J/\psi} \lesssim \mu \lesssim 2m_{J/\psi}$ , see Fig. 6. We thus select  $\mu^2 = (m_{J/\psi})^2 \approx 10 \text{ GeV}^2$  as the default scale.

## II. PHENOMENOLOGICAL MODEL

Here we consider another pion GPD model constructed in [26] called the ‘phenomenological’ model. The two models (algebraic and phenomenological) treat gluons and sea quarks at small- $x$  very differently. In the forward limit, at low renormalization scales  $\mu^2$ , the algebraic model features a strong rise of the gluon PDF at small- $x$   $G(x) \sim x^{-3/2}$ , while in the phenomenological model the growth is minimal  $G(x) \sim 1/x$ . Therefore, one might expect that the actual pion GPDs fall between these models. However, the phenomenological model is disfavored as we explain below.

Fig. S2 shows the truncation error (11) of the leading order amplitudes in the phenomenological model to be compared with Fig. 3. At  $\mu^2 = 2 \text{ GeV}^2$  (left plot), the threshold approximation is good for strange quarks but marginally acceptable for gluons. This is due to the aforementioned slow growth of gluons at small- $x$ , hence also in the central region  $|x| < \xi$ , making the imaginary part  $H^g(\xi, \xi)$  relatively non-negligible. However, the situation improves

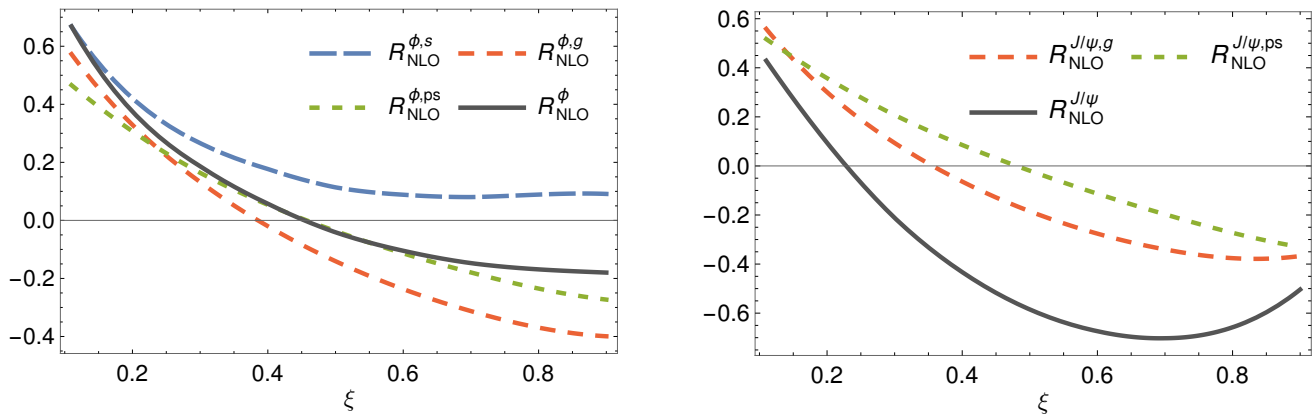


FIG. S3: Truncation error (11) of the full NLO amplitude in the phenomenological model. Left:  $\phi$ -electroproduction at  $\mu^2 = 10$   $\text{GeV}^2$ . Right:  $J/\psi$ -photoproduction at  $\mu^2 = 10$   $\text{GeV}^2$ .

at  $\mu^2 = 10$   $\text{GeV}^2$  (right plot) since the evolution enhances the gluon density in the region  $|x| < \xi$ . Next, we plot the truncation error in the full NLO amplitudes in Fig. S3. The threshold approximation in  $\phi$ -electroproduction (left plot) is acceptable, although not as good as for the algebraic model in Fig. 4. On the other hand, the approximation fails in  $J/\psi$ -photoproduction (right plot). This is because of a large cancellation between the gluon and quark terms in (S24) which makes the denominator of (11) small. Although the quark terms only appear at NLO, it is numerically important because of the unusually small gluon momentum fraction  $A_\pi^g(2 \text{ GeV}^2) \approx 0.23$  of this model. A recent lattice QCD calculation [30] points to a much larger value  $A_\pi^g(2 \text{ GeV}^2) \approx 0.54$ . We thus expect that the failure of the phenomenological model does not generalize to more realistic models. (Note that  $A_\pi^g(2 \text{ GeV}^2) \approx 0.41$  in the algebraic model.) Still, this example highlights the significance of NLO corrections and illustrates how the threshold approximation can fail due to an accidental cancellation.